Electronic supplementary information

Caterpillar-like Ag-ZnO-C Hollow Nanocomposites for Efficient Solar Photocatalytic Degradation and Disinfection

Ying Liu, Yucai Wan, Chuncai Kong, Pan Cheng, Qin Cheng, Qiongzhen Liu, Ke Liu, Ming Xia, Qihao Guo, Dong Wang**

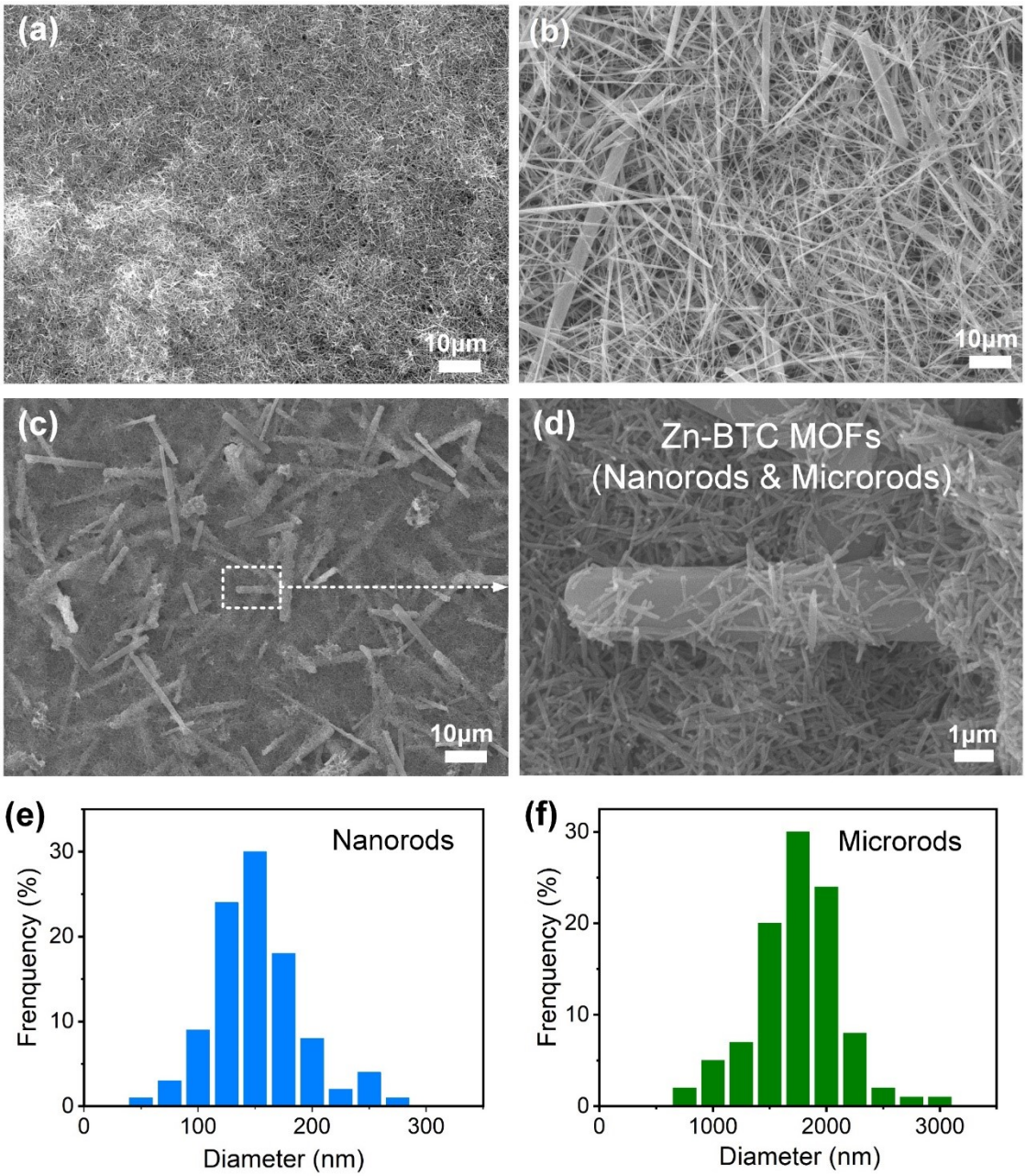

Figure S1. SEM images of Zn-BTC MOF rods synthesized with different reaction time. (a) 5min, (b) 15min, (c) 30min and (d) the enlarged image of (c) room temperature. Diameter distribution of (e) nanorods and (f) microrods of Zn-BTC MOFs statistically analyzed from (c) and (d) using e-Ruler software.

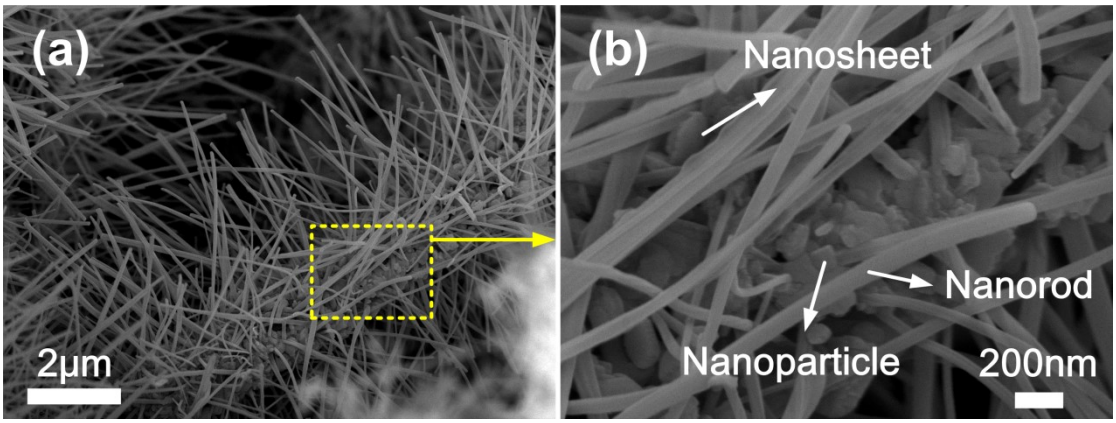

Figure S2. SEM images of Zn-BTC MOFs derivatives obtained at 550 °C. (a) hierarchical microcluster, (b) nano-components in the microcluster.

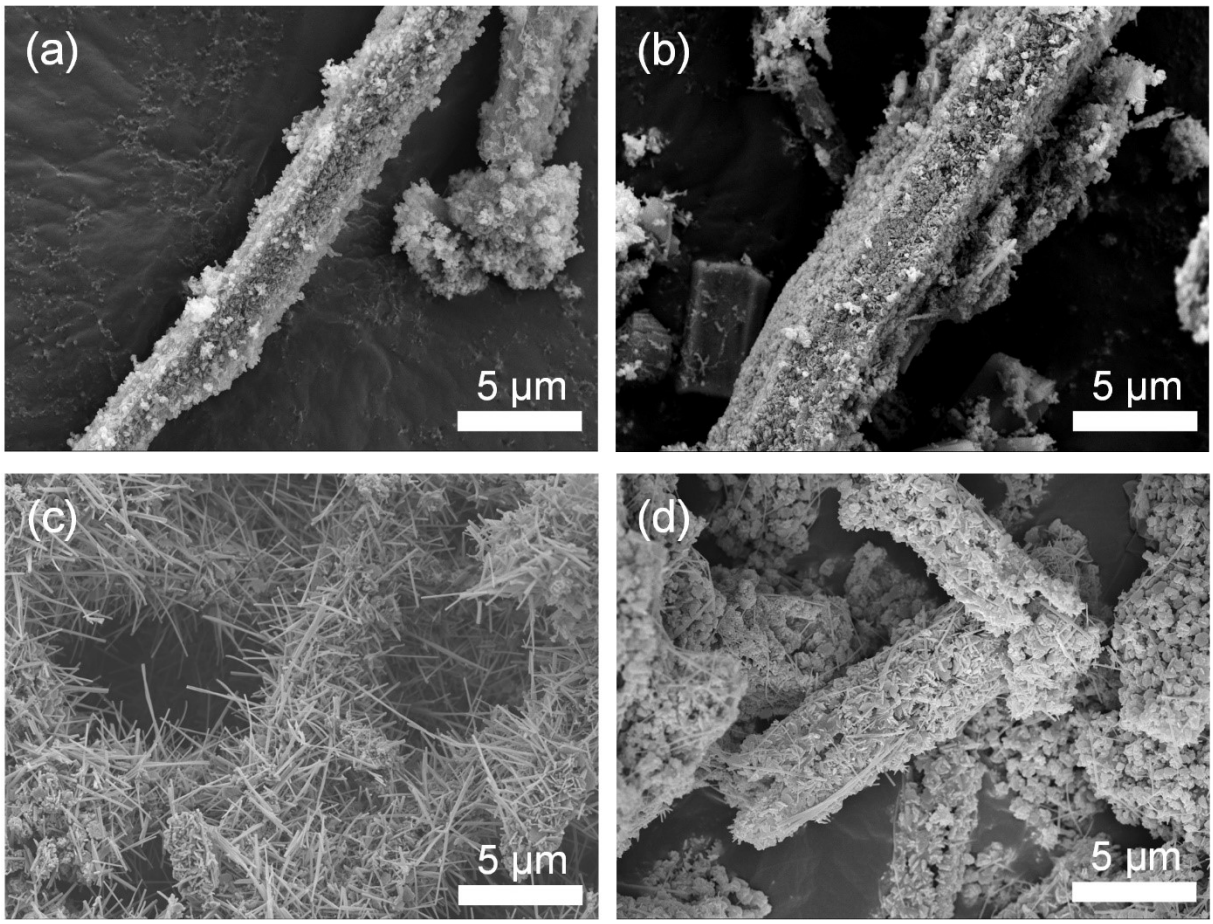

Figure S3. SEM images of Zn-BTC MOFs derivatives obtained at different temperatures (a) 450 °C, (b) 500 °C, (c) 550 °C, (d) 600 °C.

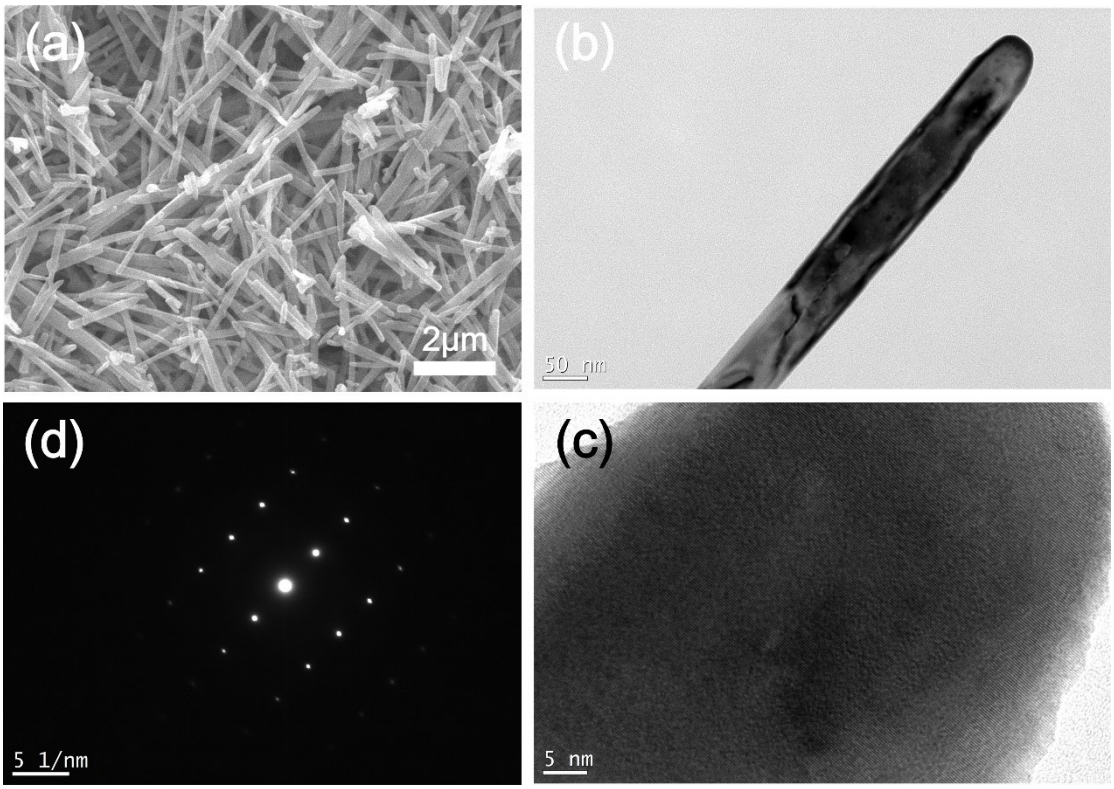

Figure S4. (a) SEM image of ZnO nanorods control, (b) TEM image, (c) HRTEM image and (d) selected area electron diffraction (SAED) pattern of typical single ZnO nanorod.

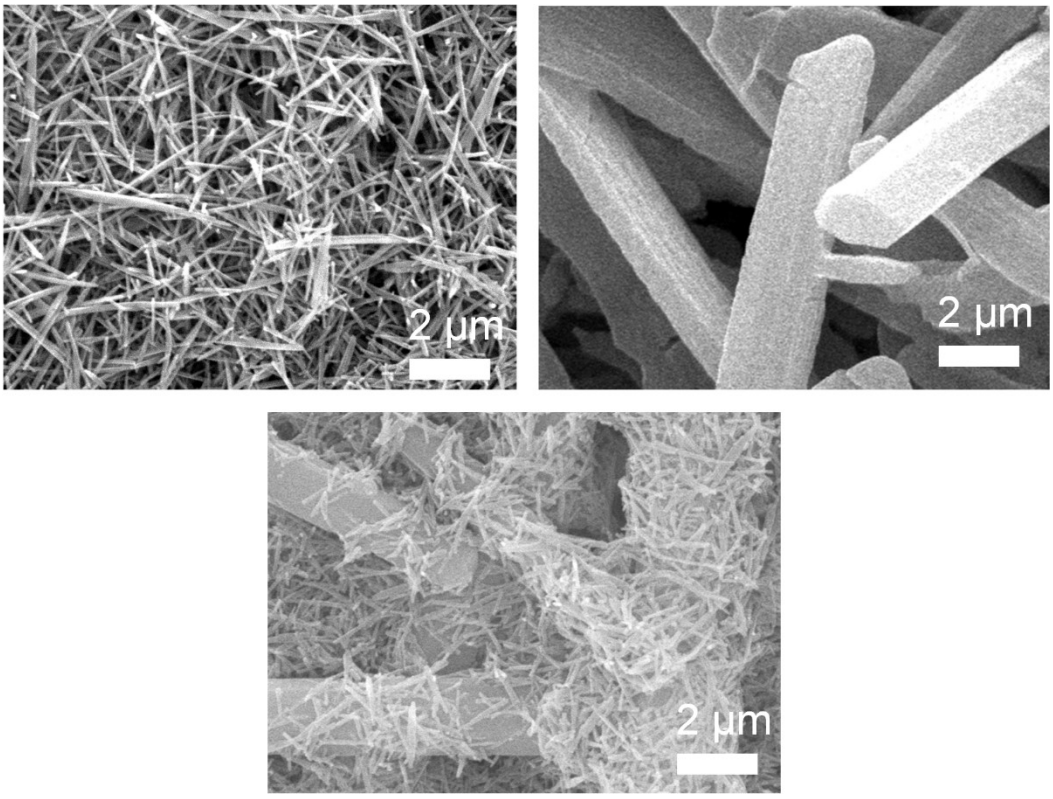

Figure S5. SEM images of Zn-BTC MOFs rods with different size. (a) nanorods (Zn-BTC-nano), (b) microrods (Zn-BTC-micro), (c) micro&nanorods (Zn-BTC).

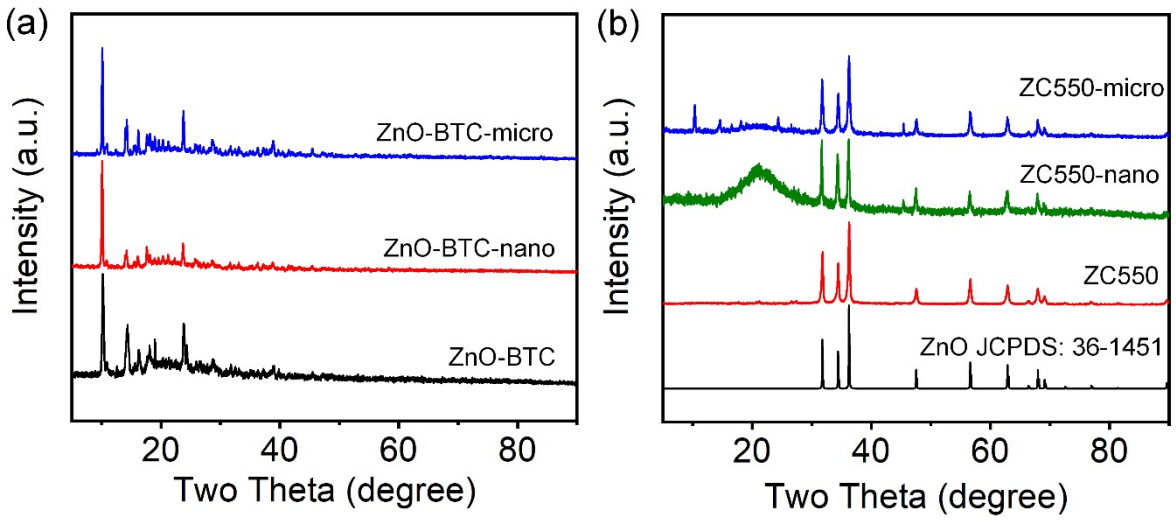

Figure S6. XRD patterns of (a) Zn-BTC-micro, Zn-BTC-nano, Zn-BTC, and (b) their derivatives: ZC550-micro, ZC550-nano, ZC550.

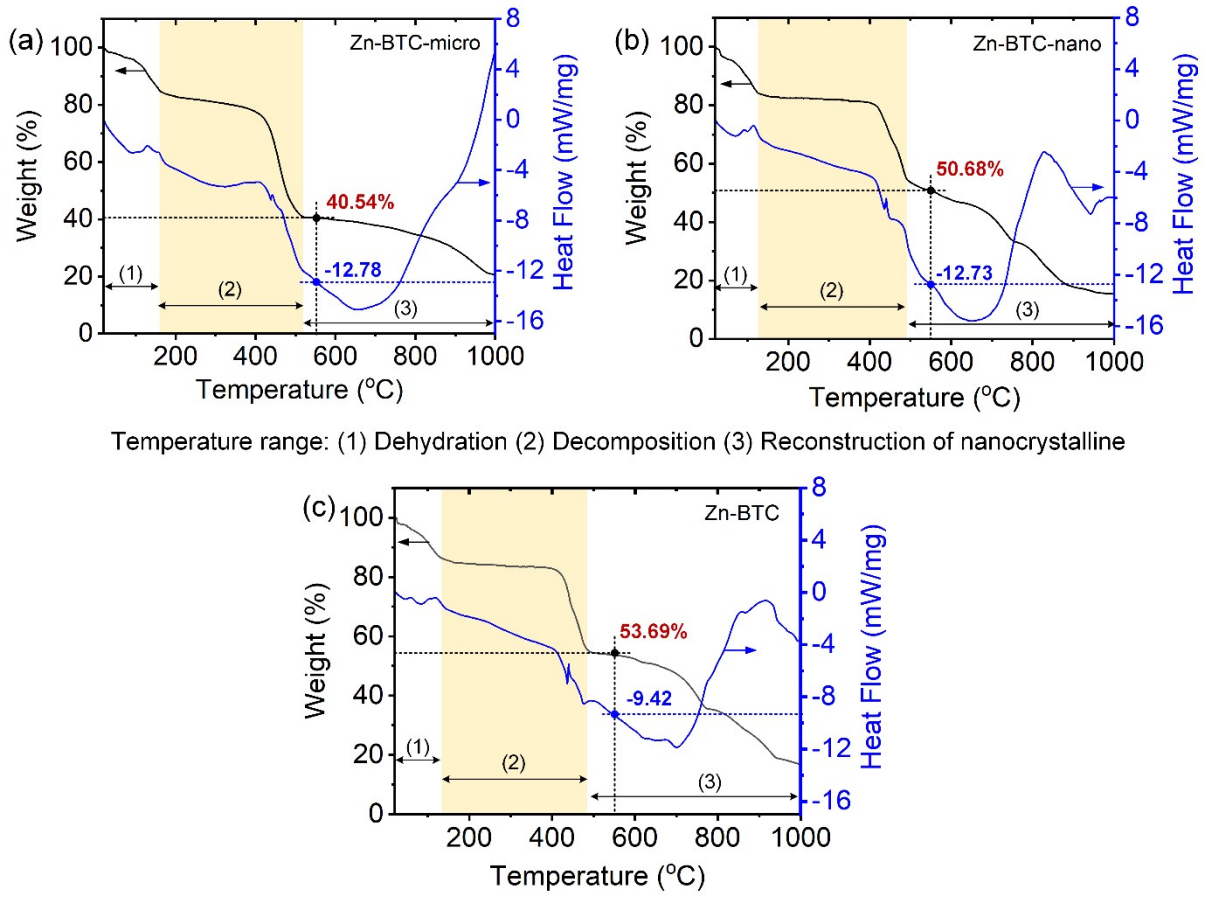

Figure S7. TG and DSC curves of (a) Zn-BTC-micro, (b) Zn-BTC-nano, (c) Zn-BTC.

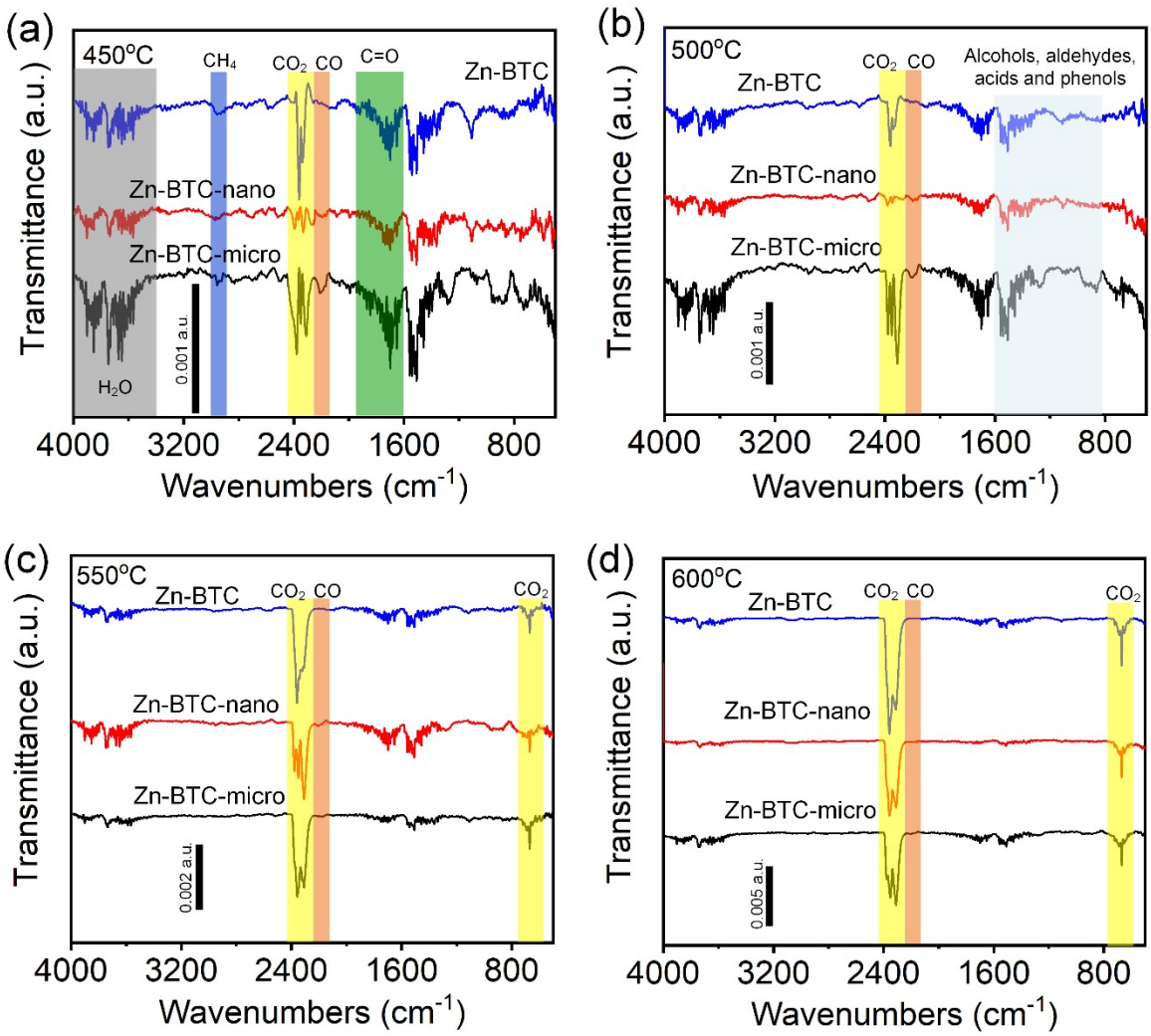

Figure S8. FTIR spectra of gas relased during heat treatment at (a) 450 °C, (b) 500 °C, (c) 550 °C, (d) 600 °C.

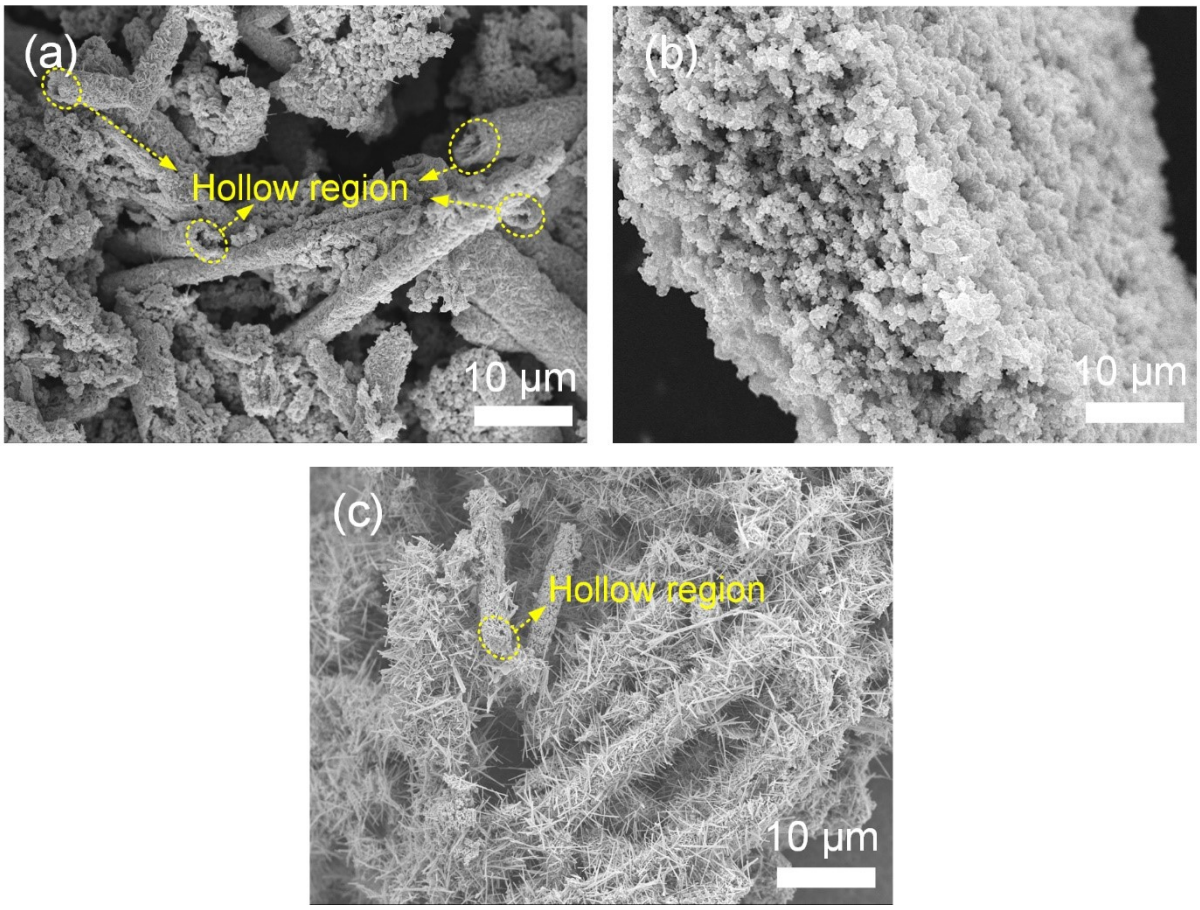

Figure S9. SEM images of (a) ZC550-micro, (b) ZC550-nano, (c) ZC550.

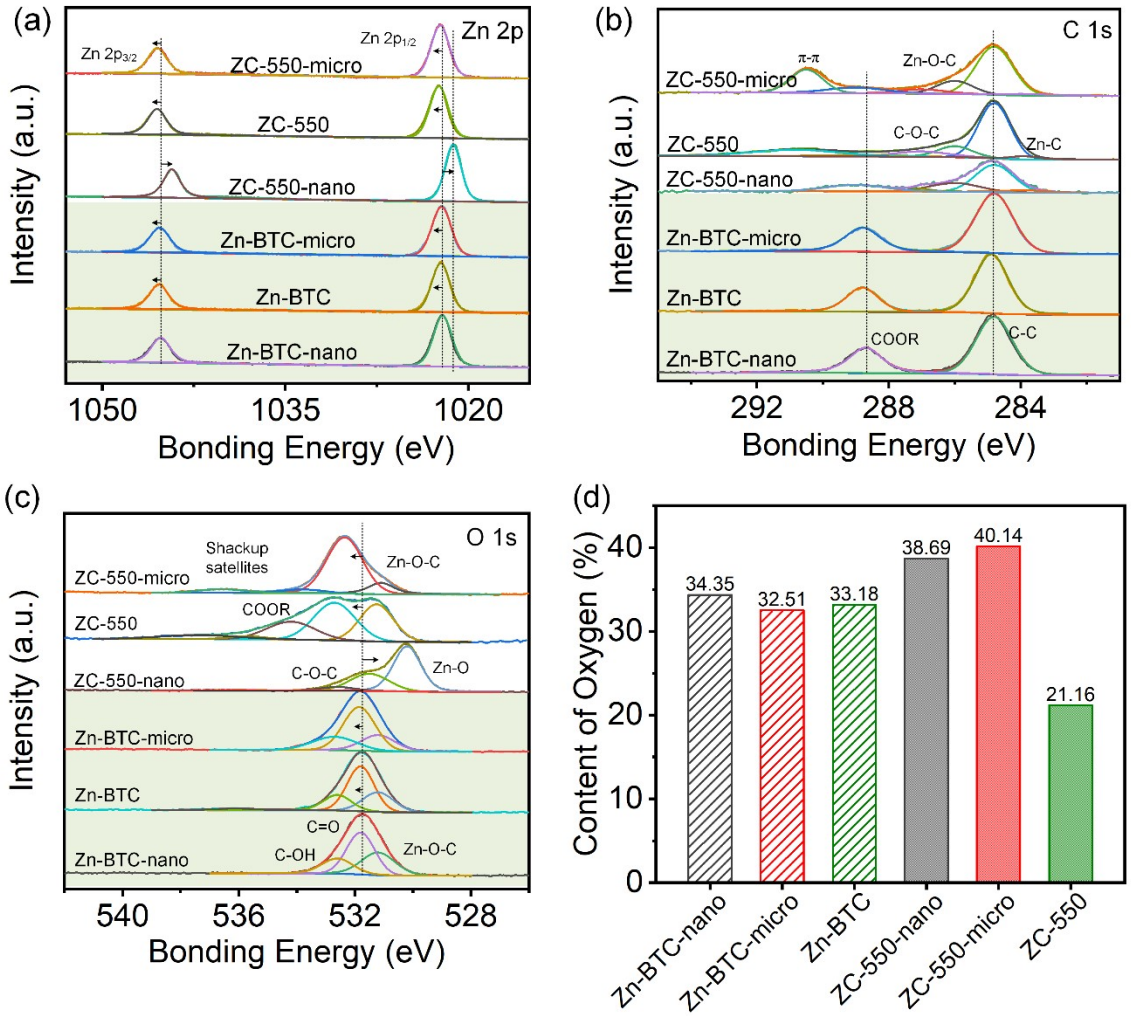

Figure S10. XPS spectra of (a) Zn2p, (b) O1s, (c) C1s and (d) content of oxygen of specimens: Zn-BTC-micro, Zn-BTC-nano, Zn-BTC, and their derivative: ZC550-micro, ZC550-nano, ZC550.

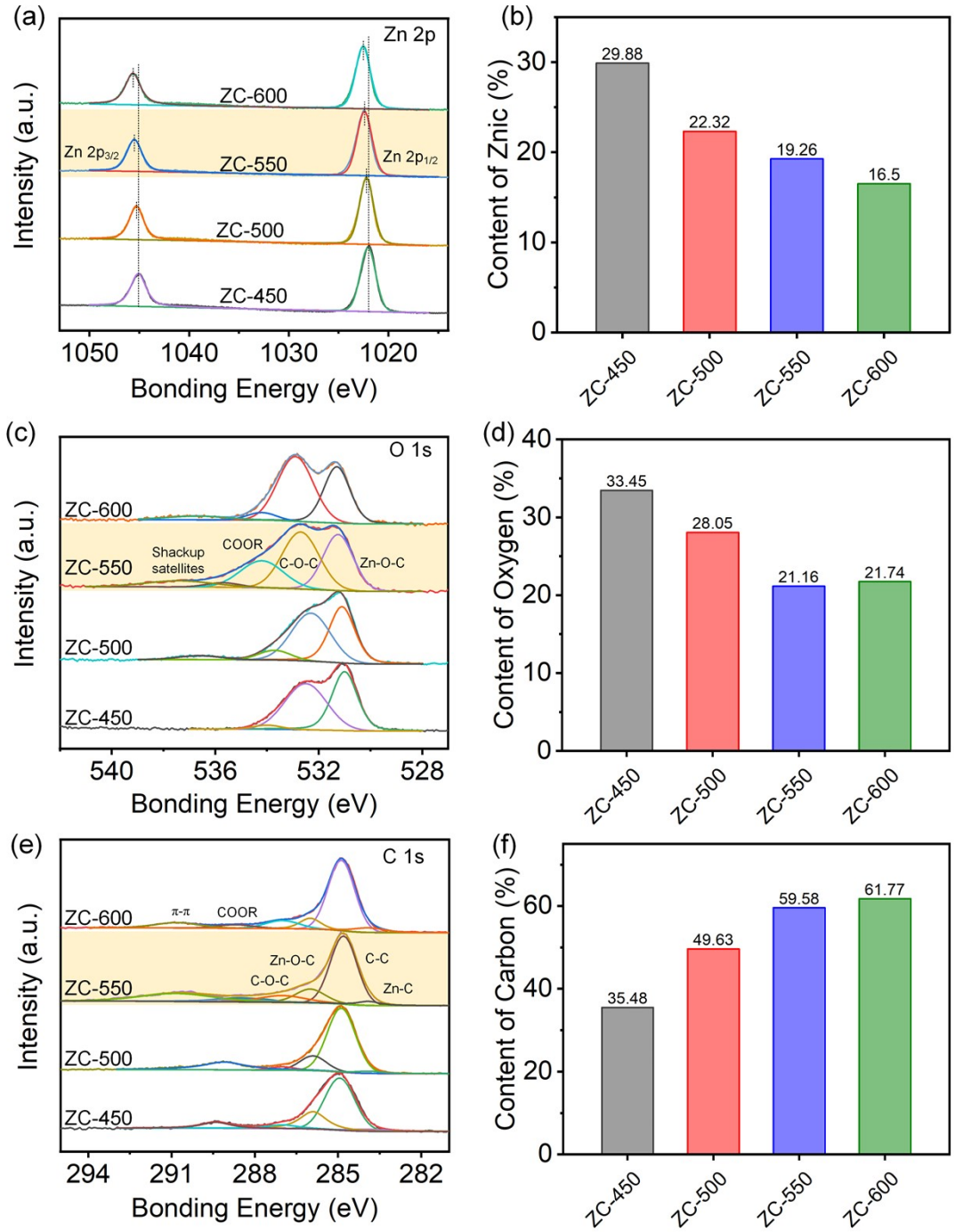

Figure S11. XPS spectra of (a) Zn2p, (c) O1s, (d) C1s and the content of (b) znic, (d) oxygen, and (f) carbon of specimens: ZC450, ZC500, ZC550, ZC600.

Table S1. Surface and pore parameters of ZnO, Zn-BTC and its derivatives.

	[a]BET specific surface area (m^2/g)	[b]Total pore volume (cm^3/g)	[c]Micropore volume (cm^3/g)	[d]Pore size (nm)
ZnO	6.07	0.025	----	28.6018
Zn-BTC	13.26	0.042	0.000178	31.5082
ZC450	28.07	0.035	0.008823	10.0242
ZC500	160.59	0.121	0.058385	5.5376
ZC550	**256.58**	**0.243**	**0.066586**	**5.4504**
AZC550	**289.79**	**0.203**	**0.042580**	**3.4861**
ZC600	205.28	0.177	0.058374	4.6724
AZC600	255.41	0.240	0.059086	4.7996

[a] The BET surface area was calculated from the linear part of the BET plot (P/P0=0.1-0.3).
[b] Total pore volume was determined by adsorption branch of the nitrogen isotherms at P/P0=0.97.
[c] Micropore volume was determined by adsorption branch of the nitrogen isotherms at P/P0=0.97.
[d] Average pore size was estimated using the adsorption branch of the nitrogen isotherms and the Barrett-Joyner-Halenda method.

Table S2. The element content in ZnO, ZC550 and AZC550 obtained from XPS.

Specimen	Atomic %			
	Zn	O	C	Ag
ZnO	54.21	45.79	0	0
ZC550	19.26	21.16	59.58	0
AZC550	15.68	20.47	60.62	3.23

Reaction rate constant

The photocatalytic activity was accurately described by pseudo-first order kinetic model determined according to Equation (S1) [1]:

$$\ln\left(C_0/C\right) = kt + \ln\left(C_0/C_1\right) \quad \text{(S1)}$$

where k is the reaction rate constant, C_0 is the initial concentration of pollutant, C_1 is the concentration after adsorption, and C is the MB concentration at irradiation time t. The value of ln (C_0/C_1) represents the adsorption efficiency of photocatalyst for pollutant molecules, the fitting curves for the plots of ln(C_0/C) are coerced to go through the intercepts of ln(C_0/C_1) in the y-axis [1]. The results of rate constants k are shown in Figure S9.

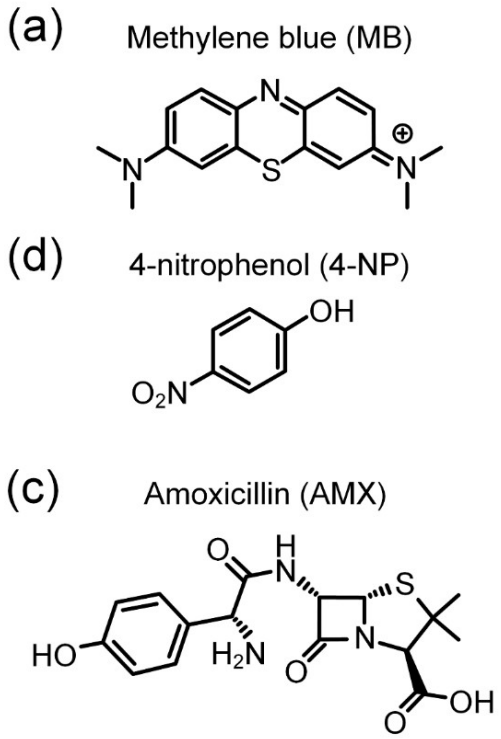

Figure S12. Molecular formula of (a) methylene blue, (b) 4-nitrophenol, and (c) amoxicillin.

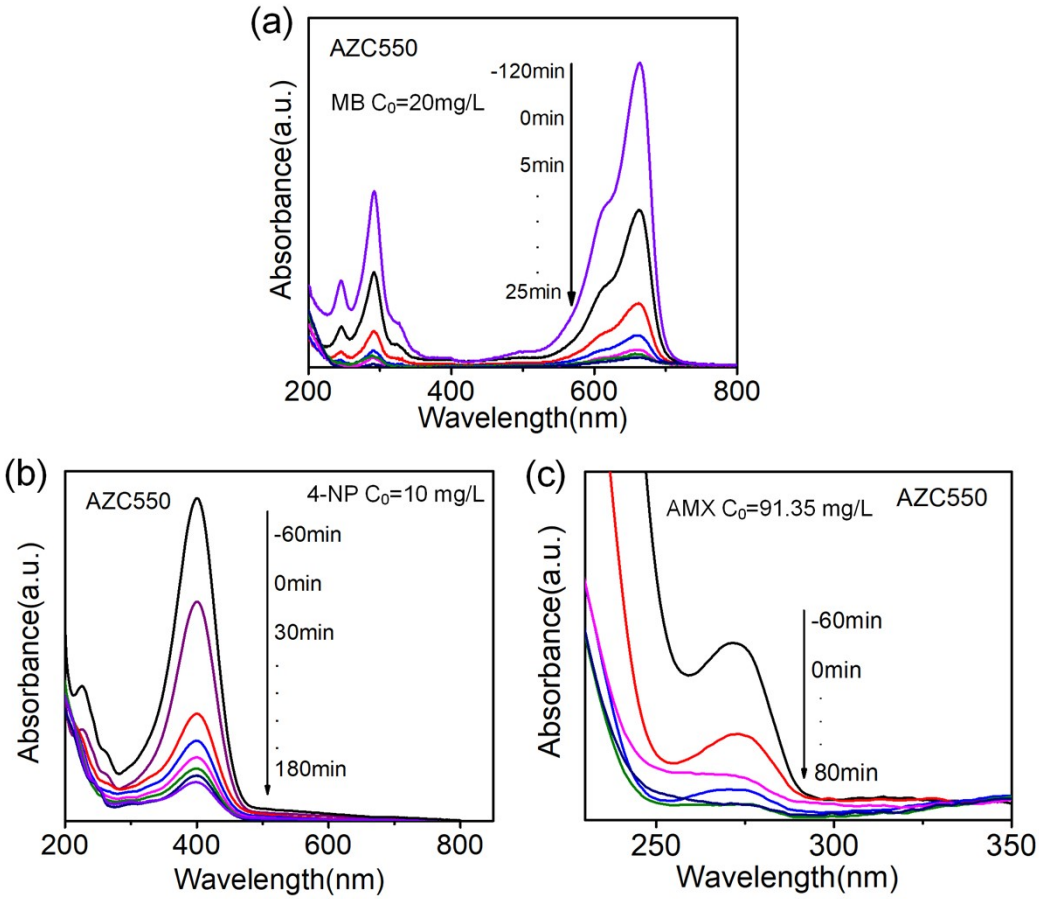

Figure S13. UV-vis absorption spectra of (a) MB (C_0=20 mg/L), 4-NP (C_0=10 mg/L)and AMX (C_0=91.35 mg/L) adsorbed and photodegraded by AZC550 at different time intervals.

Table S3. Zeta potential of ZnO, ZC550 and AZC550 at pH=7.

Specimen	ZnO	ZC550	AZC550
Zata potential (mV)	+15.5	-36.3	-20.4

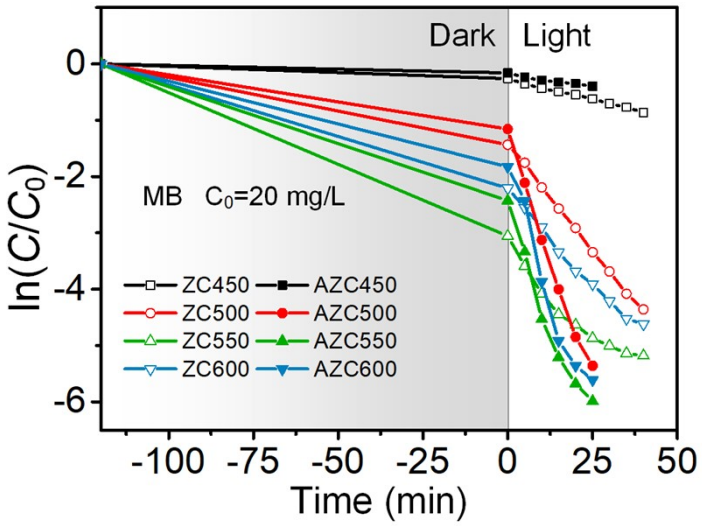

Figure S14. Time-course variation of ln(C/C_0) of MB degraded by ZC and AZC samples.

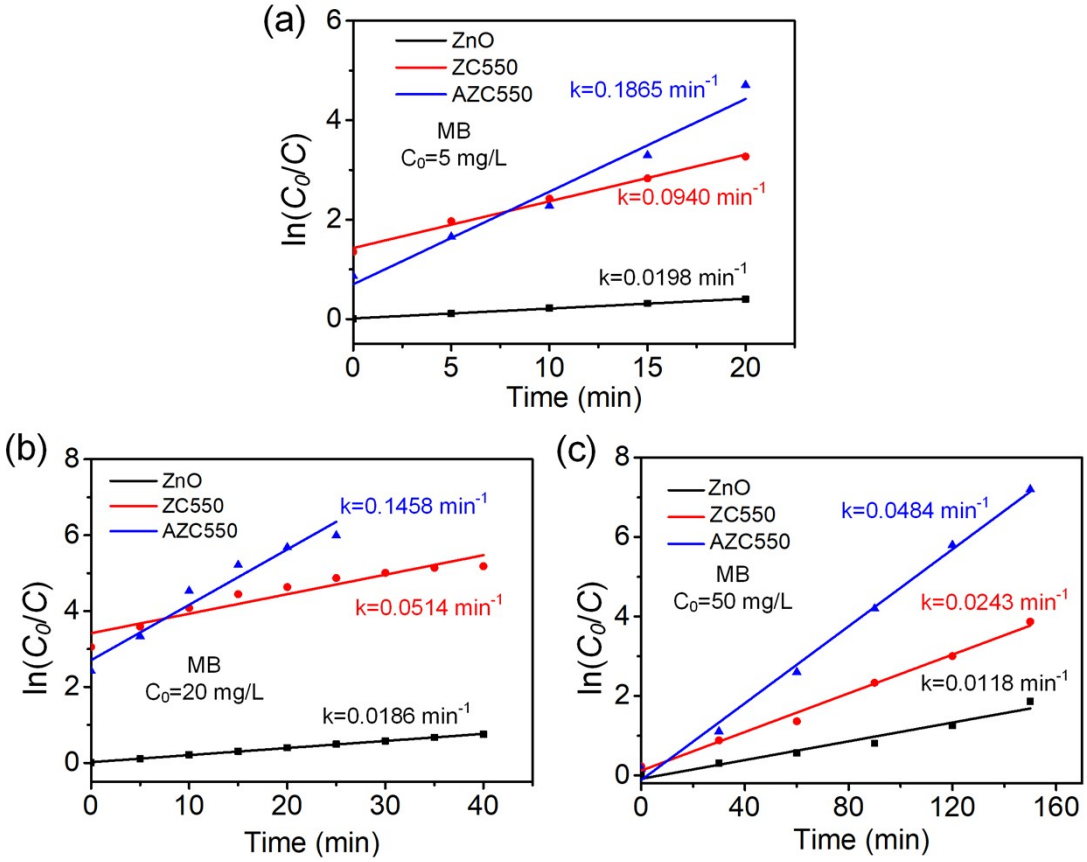

Figure S15. Time-course variation of ln(C_0/C) of MB degraded by ZnO, ZC550 and AZC550 at different C_0 of MB: (a) 5 mg/L, (b) 20 mg/L, (c) 50 mg/L.

Preparation of ZnO/C and Ag-ZnO/C control

In the process, 0.0138g of $AgNO_3$ was added into 50 mL deionized water and stirred to a stable solution. Then 1g ZnO nanorods black powder was further immersed into above solution and dispersed well with the assistance of ultrasonic wave. Next, the suspension was then kept in a transparent small beaker, which was exposed under a hernia lamp (300 W) for 1h with the light intensity set as 100 mW/cm^2. Then, Ag-ZnO black powder control was collected as catalyst after cleaned by deionized water for three times. Additionally, active carbon was prepared by pyrolyzing BTC powder at 550 ^oC for 2h. Finally, Ag-ZnO/C was obtained by mixing Ag-ZnO powder with active carbon powder thoroughly with atomic ratio of zinc to carbon 1:3.

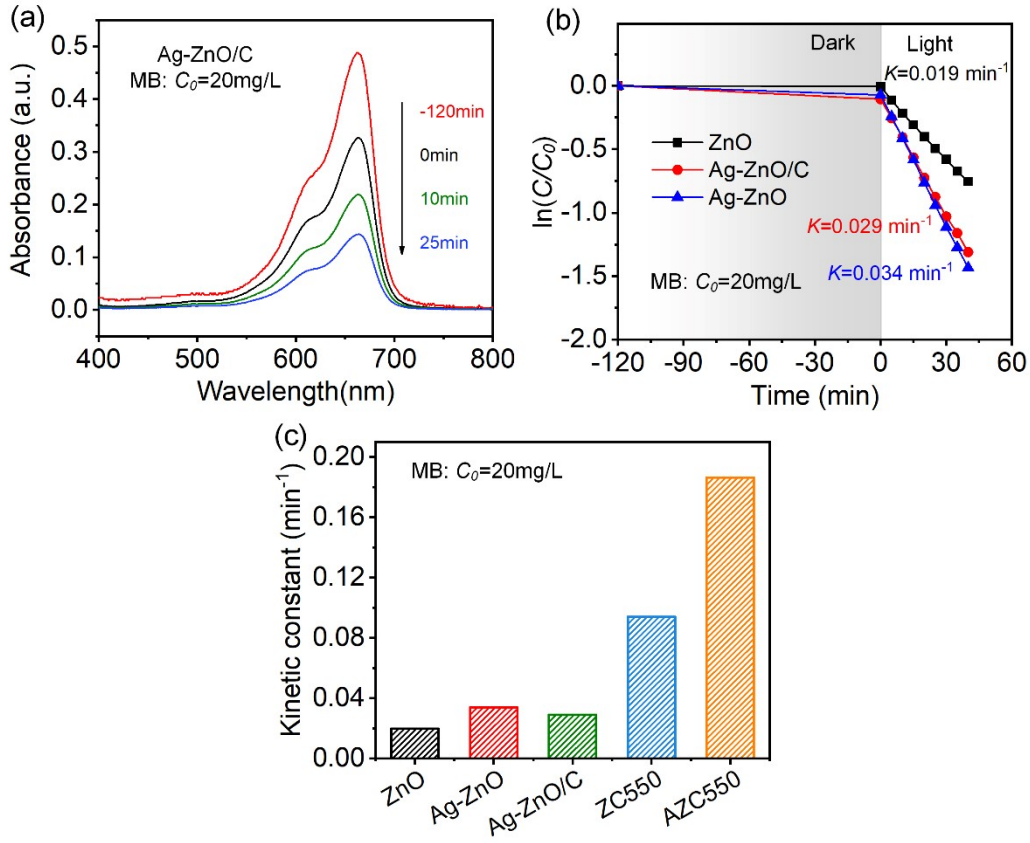

Figure S16. Catalytic performance of mixture control: Ag-ZnO/C. (a) UV-vis absorption spectra of MB (C_0=20 mg/L) adsorbed and photodegraded by control at different time intervals; (b) Time-course variation of ln(C/C_0) of MB degraded by Ag-ZnO/C compared with ZnO and Ag-ZnO; (c) Kinetic constant of photodegrading MB with initial concentration of 20 mg/L over ZnO, Ag-ZnO, Ag-ZnO/C, ZC550 and AZC550

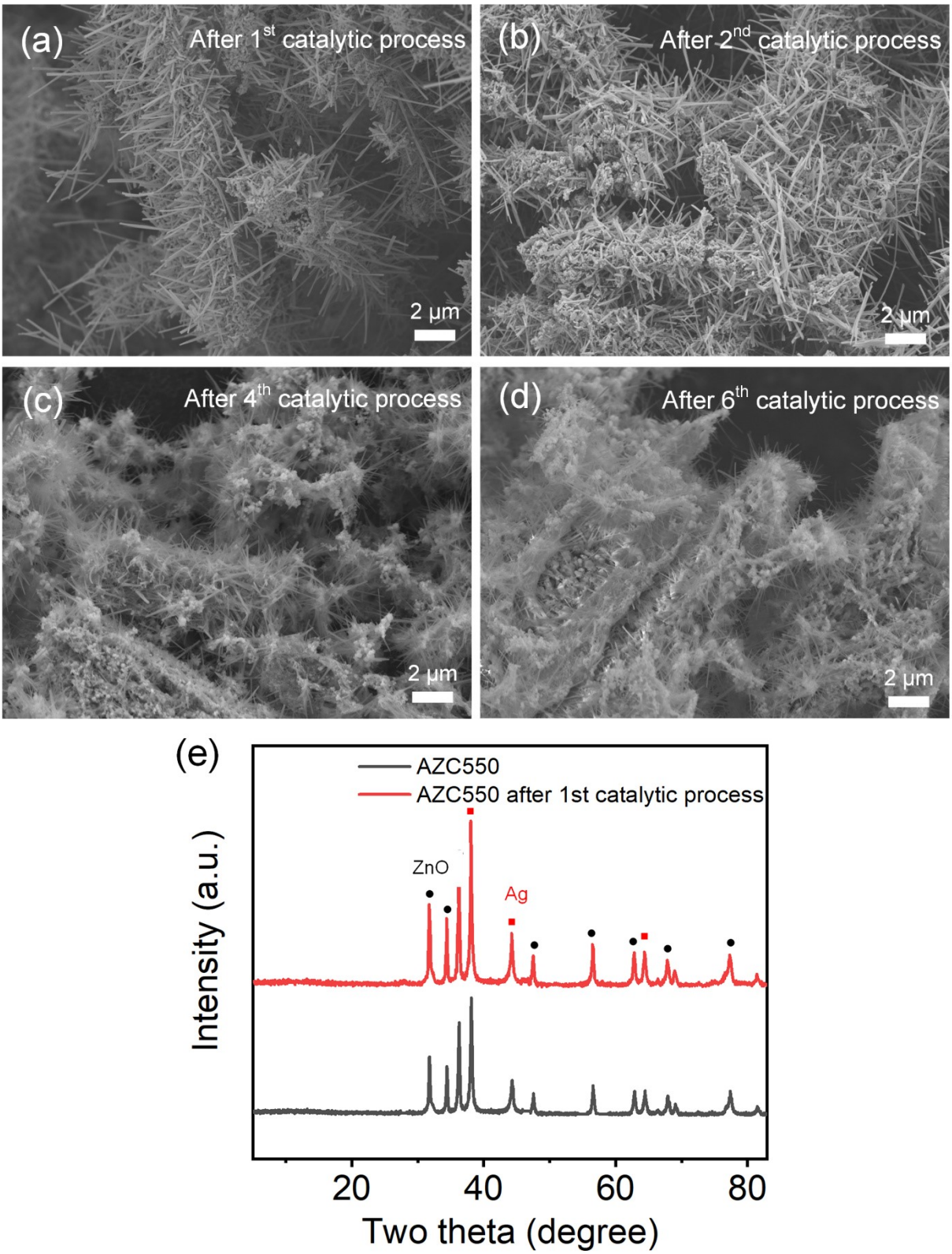

Figure S17. SEM images of AZC550 after photocatalytic degradation process of 20 mg/L MB. (a) 1st round, (b) 2nd round, (c) 4th round, (d) 6th round and (e) XRD of AZC550 before and after catalytic process.

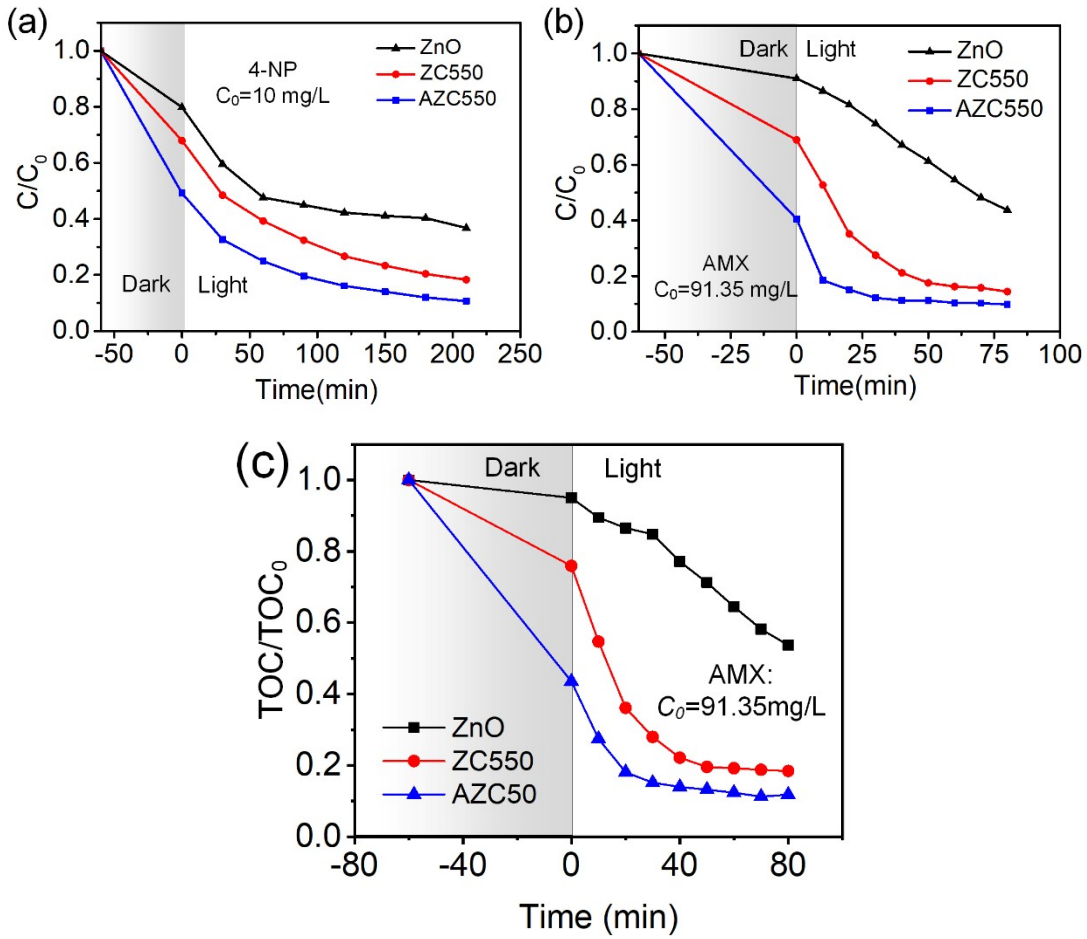

Figure S18. Time-course variation of C/C_0 of (a) 4-NP and (b) AMX; (c) time depended TOC value of AMX degraded by catalysts.

Analytical measurements and by-products identification

Degradation byproducts of amoxicillin produced during their photo-induced degradation were monitored by an UHPLC Dionex Ultimate 3000 with Q-Exactive hybrid quadrupole-orbitrap mass spectrometer system (Ultimate 3000 UHPLC-Q Exactive, Thermo Scientific, US). Chromatographic peaks were separated on a Kinetex EVO C18 column (2.1 mm × 100 mm, 2.6μm, 100 Å) at a flow rate of 0.2 mL/min with gradient acetonitrile containing 0.1% acetate(A) and water containing 0.1% acetate (B) as follows: 0-3 min, 5% A,3-3.1min,5-50%A, 3.1-13 min, 50% A, 13-13.1min, 50-75%A, 13.1-18min, 75% A, 18-18.1min, 75-5% A. The injection volume was 5 μL for analysis. The Q-Exactive mass spectrometer was equipped with heat electrospray ionization (HESI), an online vacuum degasser, a quaternary pump, an autosampler and a thermostated column compartment. The optimized parameters of mass spectrometry were illustrated as below: spray voltage: + 3.0 kV ; sheath gas pressure: 40 ml/min; aux gas pressure: 10 ml/min; capillary temperature: 300 °C; S-lens: 50 V; scan mode: (1) Positive ion full MS: resolution: 70000; scan range: 50-750 m/z; (2) dd-MS2/dd-SIM: resolution: 17500; the initial ion 50 m/z.

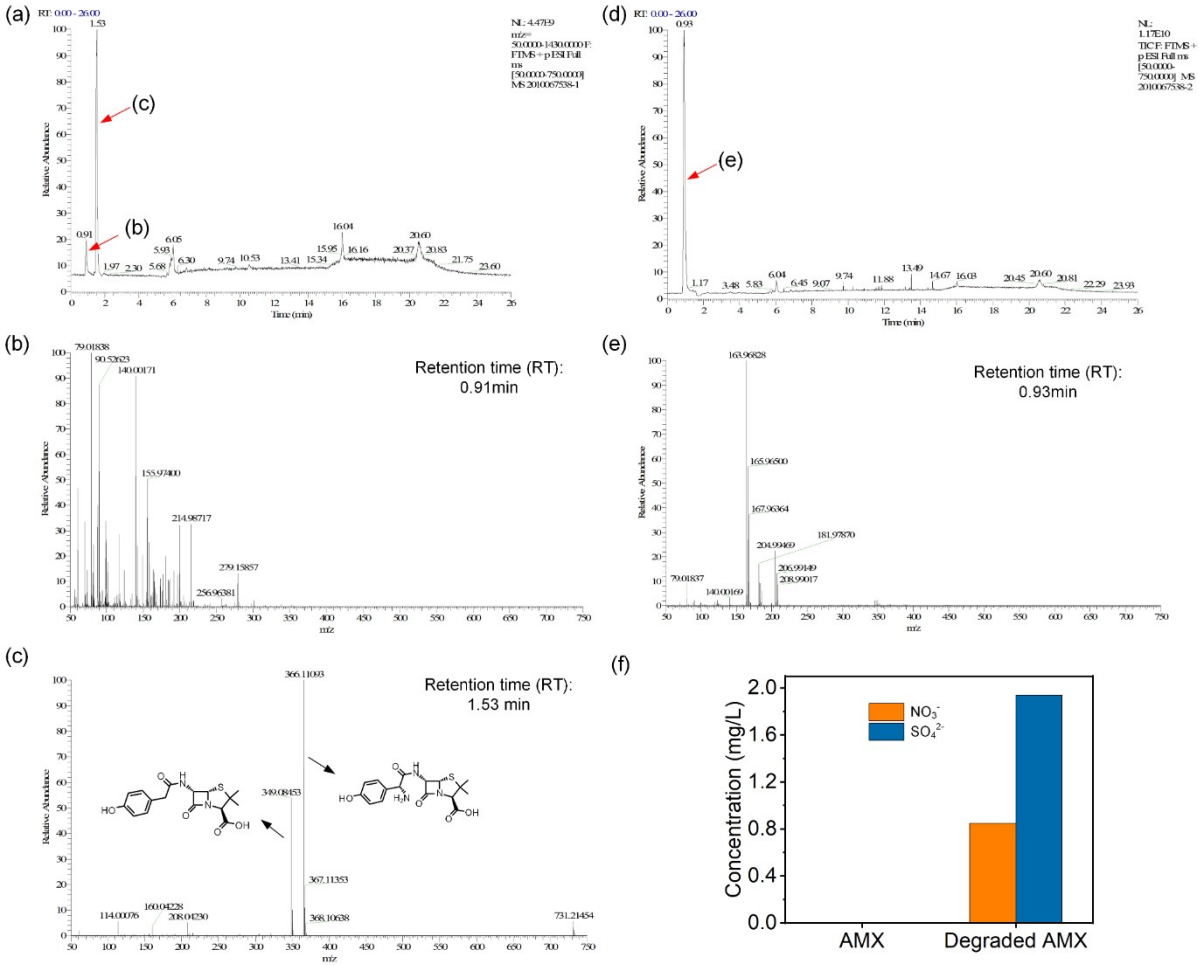

Figure S19. UHPLC-UV chromatograms of (a) AMX solution and (d) AMX with AZC550 irradiated for 80 min; MS/MS product-ion mass spectra of AMX solution at (b) RT=0.91 min and (c) RT=1.53 min; (e) MS/MS product-ion mass spectra of AMX with AZC550 irradiated for 80 min at RT=0.93 min; (f) concentration of NO^- and SO_4^{2-} in AMX solution before and after photodegradation obtained by ion chromatography measurement.

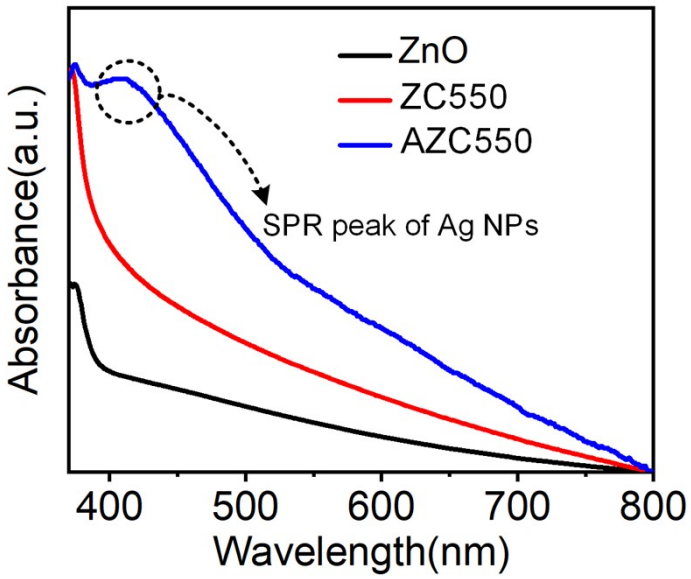

Figure S20. UV-vis diffuse reflectance spectra (DRS) of AZC550 compared to ZnO and ZC550.

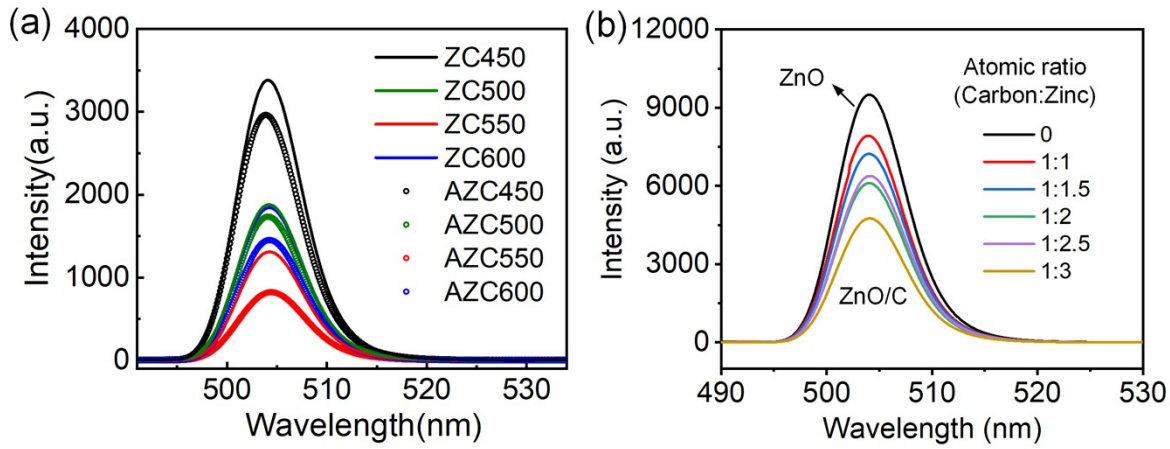

Figure S21. PL spectra of (a) ZC and AZC catalysts, (b) ZnO/C (mixture of ZnO nanorods and BTC derived active carbon) with atomic ratio of carbon to Zinc from 0 to 3:1.

Photo-electrochemical measurements

Transient photocurrent response and electrochemical impedance spectroscopy (EIS) measurements were conducted on a CHI660E electrochemical workstation with standard three-electrode cell at room temperature. The as-prepared photocatalysts were deposited on glass carbon electrode with the diameter of 4 mm to prepare the working electrode. Platinum (Pt) wire was utilized as a counter and saturated calomel electrode (SCE) as a reference electrode in 0.50 M Na_2SO_4 aqueous solution electrolyte. A 300 W xenon arc lamp with UV cut-off filter $\lambda > 420$ nm was employed as an excitation source at the external voltage of 0.50 V.

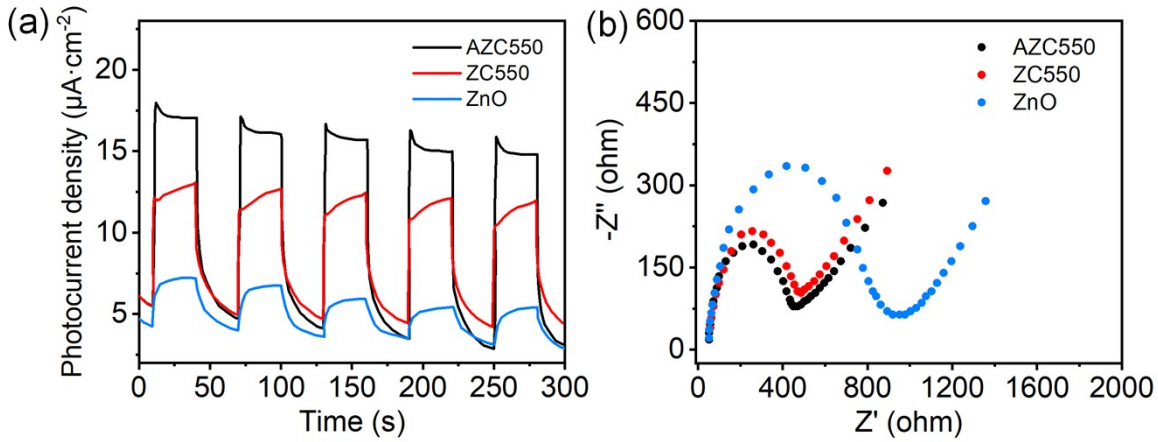

Figure S22. (a) Transient photocurrent responses and (b) EIS Nyquist plots of ZnO, ZC550, and AZC550.

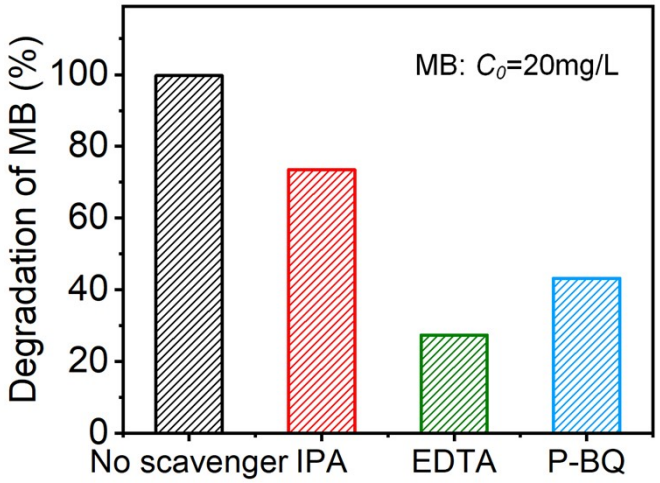

Figure S23. Active species trapping experiments of AZC550 toward the degradation of MB with initial concentration of 20mg/L under visible light irradiation.

Table S4. Comparison of the photocatalytic degradation capacities of various catalysts reported in the literature for the reduction of MB, 4-NP and AMX.

Pollutant	Catalyst		Pollutant		Light source (power, mW/cm^2) **	TOF* (10^{-3}mol/mol/min)
	Catalyst	Dosage (mg)	concentration (mg/L)	Dosage (mL)		
MB	AZC550	5	20	15	VL (100)	3.00
	Ag-ZnO[2]	5	10	15	VL (31)	0.41
	ZnO[3]	5	10	15	VL	0.28
	ZIF-8[4]	5	10	15	UV***	0.17
	ZnO[5]	5	20	15	VL	0.25
4-NP	AZC550	5	10	15	VL (100)	0.14
	Ag-ZnO-C[6]	5	5	15	VL	0.05
	Ag-ZnO[7]	5	10	15	VL (100)	1.30
	ZnO[3]	5	5	15	VL	0.16
	g-C_3N_4-ZnO[8]	5	4	15	VL	0.004
	Ag-ZnO[2]	5	5	15	VL (31)	0.13
AMX	AZC550	5	91.35	15	VL (100)	3.43
	UV/ZnO[9]	5	104	15	UV	1.16
	Fe_3O_4/g-C_3N_4[10]	5	91.35	15	UV	2.78
	TiO_2[11]	5	41.94	15	UV	0.53
	NH_2-MOF-Sm_2O_3-ZnO[12]	5	300	15	UV	5.55
	p-CuO/n-ZnO[13]	5	50	15	VL (109)	0.40

*TOF=the mole of pollutant per mole of catalyst per second when pollutant reached full (100%) conversion (Time recorded from the adsorption of pollutant).

**VL=Visible light, UV=UV irradiation

References:

[1] S. Liu, F. Li, Y. Li, Y. Hao, X. Wang, B. Li, R. Liu, *Applied Catalysis B: Environmental* **2017**, 212, 115.

[2] S. A. Ansari, M. M. Khan, M. O. Ansari, J. Lee, M. H. Cho, *The Journal of Physical Chemistry C* **2013**, 117, 27023.

[3] S. A. Ansari, M. M. Khan, S. Kalathil, A. Nisar, J. Lee, M. H. Cho, *Nanoscale* **2013**, 5, 9238.

[4] H. Jing, C. Wang, Y. Zhang, P. Wang, R. Li, *RSC Advances* **2014**, 4, 54454.

[5] C. Yu, Z. Tong, S. Li, Y. Yin, *Materials Letters* **2019**, 240, 161.

[6] S. Y. Sawant, J. Y. Kim, T. H. Han, S. A. Ansariab, M. H. Cho, *New Journal of Chemistry* **2018**, 42, 1995.

[7] H. Mou, C. Song, Y. Zhou, B. Zhang, D. Wang, *Applied Catalysis B: Environmental* **2018**, 221, 565.

[8] J. Sun, Y. Yuan, L. Qiu, X. Jiang, A. Xie, Y. Shen, J. Zhu, *Dalton Transactions* **2012**, 41, 6756.

[9] E. S. Elmolla, M. Chaudhuri, *Journal of Hazardous Materials* **2010**, 173, 445.

[10] A. Mirzaei, Z. Chen, F. Haghighat, L. Yerushalmi, *Applied Catalysis B: Environmental* **2019**, 242, 337.

[11] L. Bergamonti, C. Bergonzi, C. Graiff, P. P. Lottici, R. Bettini, L. Elviri, *Water Research* **2019**, 163, 114841.

[12] R. Abazari, A. R. Mahjoub, *Inorganic chemistry* **2018**, 57, 2529.

[13] Y. Belaissa, D. Nibou, A. A. Assadi, B. Bellal, M. Trari, *Journal of the Taiwan Institute of Chemical Engineers* **2016**, 68, 254.